PAPER

Electronic and structural characterisation of polycrystalline platinum disulfide thin films†

Kuanysh Zhussupbekov, [ID] *[ab] Conor P. Cullen,[bc] Ainur Zhussupbekova, [ID] [ab] Igor V. Shvets, [ID] [ab] Georg S. Duesberg, [ID] [d] Niall McEvoy [ID] *[bc] and Cormac Ó Coileáin [ID] *[bc]

We employ a combination of scanning tunnelling microscopy (STM) and scanning tunnelling spectroscopy (STS) to investigate the properties of layered PtS_2, synthesised *via* thermally assisted conversion (TAC) of a metallic Pt thin film. STM measurements reveal the 1T crystal structure of PtS_2, and the lattice constant is determined to be 3.58 ± 0.03 Å. STS allowed the electronic structure of individual PtS_2 crystallites to be directly probed and a bandgap of ~1.03 eV was determined for a 3.8 nm thick flake at liquid nitrogen temperature. These findings substantially expand understanding of the atomic and electronic structure of PtS_2 and indicate that STM is a powerful tool capable of locally probing non-uniform polycrystalline films, such as those produced by TAC. Prior to STM/STS measurements the quality of synthesised TAC PtS_2 was analysed by X-ray photoelectron spectroscopy (XPS) and Raman spectroscopy. These results are of relevance to applications-focussed studies centred on PtS_2 and may inform future efforts to optimise the synthesis conditions for thin film PtS_2.

1. Introduction

The investigation of new two-dimensional (2D) materials has been of increasing interest since the experimental discovery of graphene[1] with many reports focusing on their interesting and unique properties which are of great interest for both fundamental research[2–4] and applications.[5–8] Due to the absence of a natural bandgap in graphene, research attention has turned towards 2D materials with a bandgap, particularly those which are stable in ambient conditions. Transition Metal Dichalcogenides (TMDs)[9–11] are a family of 2D materials that can be of semiconducting character with a layer-dependent bandgap.[12,13] The chemical formula for TMDs is generally expressed as MX_2, where M is a transition metal and X is a chalcogen (S, Se or Te). Each discrete layer of a TMD typically consists of a hexagonal layer of the M atoms which are held between two hexagonal layers of the X atoms. The layered structure of the crystals stems from van der Waals interactions between adjacent TMD layers. TMDs can have a variety of electronic properties, such as metallic, semiconducting, and superconducting, depending on their composition, crystal structure and thickness. The properties of 2D TMDs

are often significantly different from their bulk forms and can be fine-tuned for numerous applications.[14] Due to this versatility, TMDs are poised to play important roles in the fields of electronics,[15] optoelectronics,[16] electrochemical sensors[17] and catalysis,[18] to name but a few. One of the less-explored branches of TMD materials is noble-transition-metal dichalcogenides (NTMDs),[19] (MX_2: M = Pt and Pd, and X = S, Se and Te) which are predicted to exhibit different structural and electronic properties in comparison with well-studied MoS_2.[20,21] One member of the NTMD group is platinum disulfide (PtS_2), of which ultrathin films have recently been synthesised.[22–24] Theoretical and experimental studies have revealed that the size of the bandgap in PtS_2 decreases with increasing film thickness,[23–26] going from ~1.7 eV for monolayer PtS_2 to ~0.25 eV for the bulk state. Indirect bandgaps were observed for all layer thicknesses as opposed to MoS_2 and WS_2 where the monolayer forms possess a direct bandgap.[25] Relative positioning of the valence band maximum (VBM) and conduction band minimum (CBM) with respect to the Fermi level indicates that PtS_2 is a p-type semiconductor.[23–25] Initial investigations of its properties suggest that PtS_2 holds promise for use in diverse applications including photodetectors,[27,28] electrocatalysis,[29] photocatalysis,[30] thermoelectric devices,[31] nonlinear optics and laser photonics.[32] It should be noted that while PtS_2 is a long-established material[33,34] its synthesis is not trivial. Under typical reaction conditions for the sulfurisation of Pt, the non-layered material PtS, rather than PtS_2, has been reported as the dominant product.[35] When considering the sulfurisation of Pt, the reaction parameters must be considered and carefully tuned to obtain an appreciable yield of PtS_2.[34]

a School of Physics, Trinity College Dublin, Dublin 2, Ireland. E-mail: zhussupk@tcd.ie
b AMBER Centre, CRANN Institute, Trinity College Dublin, Dublin 2, Ireland. E-mail: nmcevoy@tcd.ie; ocoilecl@tcd.ie
c School of Chemistry, Trinity College Dublin, Dublin 2, D02 PN40, Ireland
d Institute of Physics, EIT 2, Faculty of Electrical Engineering and Information Technology, Universität der Bundeswehr München, 85579 Neubiberg, Germany
† Electronic supplementary information (ESI) available. See DOI: 10.1039/d0ra07405e

Transmission Electron Microscopy (TEM) is a powerful and widely-used technique for the characterisation of 2D materials. It is capable of atomic resolution and can be used to investigate the crystal structure, as well as the presence and quantity of defects.[24,27,36] However, direct measurements of the electronic band structure are not straightforward *via* TEM. Another limit associated with TEM is the requirement of additional sample preparation, namely that the material to be investigated must first be transferred onto a TEM grid, a potentially destructive process which can introduce contaminants. Moreover, recent reports have indicated that damage by the TEM electron beam can be a problematic issue for TMDs.[37–39] On the other hand, scanning tunnelling microscopy and spectroscopy (STM/STS) are non-destructive techniques, which can be used to map morphology and probe the electronic structure of samples[40–43] and, provided a conductive pathway can be established through the sample, do not require a transfer process.

In this letter we study the electronic properties and atomic structure of PtS_2 films synthesised *via* thermally assisted conversion (TAC) of pre-deposited Pt films. The PtS_2 films were also characterised by X-ray photoelectron spectroscopy (XPS) and Raman spectroscopy. We carried out STM measurements to investigate the crystal structure of PtS_2 and determined the in-plane lattice constant to be 3.58 ± 0.03 Å. Scanning Tunnelling Spectroscopy (STS) was employed in order to probe the electronic properties of the PtS_2. From STS measurements the electronic bandgap of a 3.8 nm thick PtS_2 crystal, measured at 77 K, was determined to be around 1.03 eV.

2. Experimental

PtS_2 samples were synthesised through the TAC of pre-deposited Pt films. A 2 nm thick metal Pt film was deposited by argon-ion sputtering (Gatan Precision Etching and Coating System (PECS)) onto a conductive pyrolytic carbon (PyC) film supported on a SiO_2/Si substrate.[44]

A low-temperature STM from Createc was utilised in this study. The STM and STS measurements were conducted in ultra-high vacuum (UHV) at liquid-nitrogen temperature (77 K). Single-crystalline W tips[45] with a (001) orientation, prepared by electrochemical etching in NaOH solution, were employed. These tips were sharpened in UHV by argon-ion sputtering to remove surface oxides. All STM images were recorded in constant-current mode. While little thermal noise is expected at low temperature, it should be noted that no drift corrections have been applied to any STM images presented here. STS spectra (dI/dV) were acquired by differentiation of the current–voltage $I(V)$ spectra. Prior to and post grid STS measurements, the surface positions were verified by STM imaging to confirm the location had remained fixed.

XPS spectra were recorded using a PHI VersaProbe III instrument. Spectra were recorded at a pass energy of 26 eV with a monochromatic Al Kα (1486.6 eV) source and dual-beam charge neutralisation with charge correction to the C 1s core-level at 284.8 eV using the CasaXPS software. XRD was acquired with a Bruker D8 Discover, equipped with a mono-chromated Cu K-alpha source.
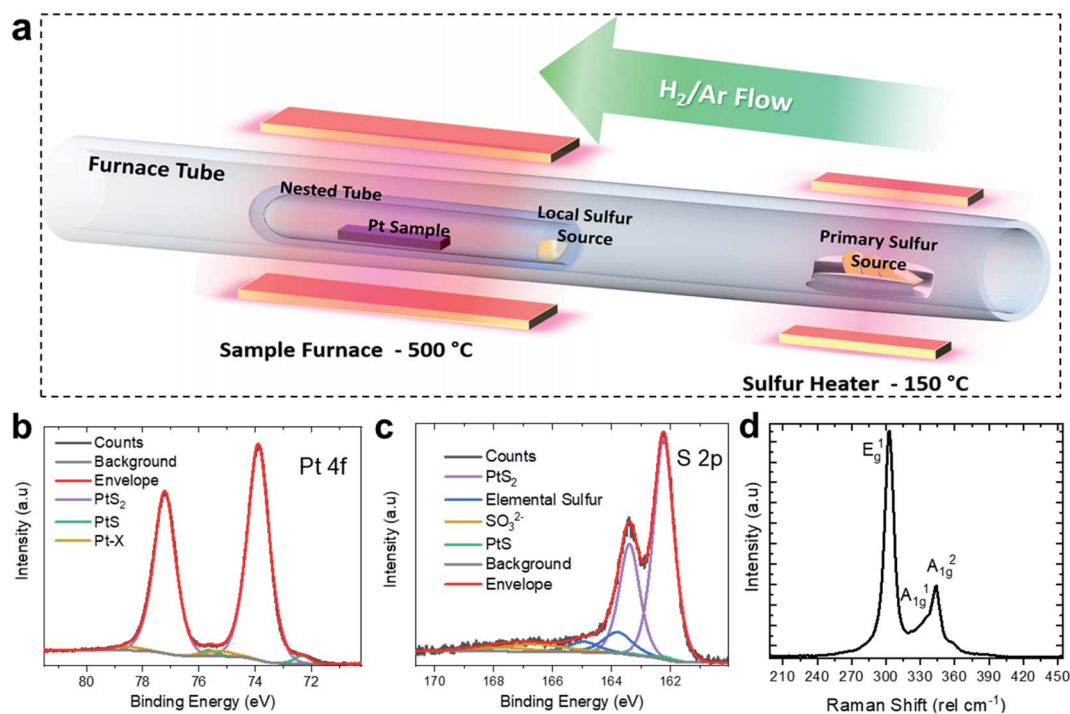

Fig. 1 Characterization of the PtS_2 film. (a) Schematic of the sulfurization process with the nested tube configuration. (b) & (c) Fitted XPS of PtS_2 film demonstrating the Pt 4f and S 2p core levels respectively. (d) Raman spectrum of a PtS_2 film presenting the three Raman–active vibrational modes. These two methods help to confirm the successful synthesis of PtS_2.

Raman spectroscopy was performed with a WITec Alpha 300 R confocal Raman microscope and a 532 nm excitation energy. Spectra were gathered by averaging across >10 discrete point spectra with a laser power < 200 μW.

3. Results and discussion

3.1. Synthesis of 1T-PtS$_2$

The synthesis of the PtS$_2$ films was performed through TAC of pre-deposited Pt films. It is notable that the synthesis temperatures of Pt-based TMDs by TAC are much lower than those associated with W or Mo films,[13,20,46,47] which lowers the thermal budget and broadens the potential application space by enabling growth on diverse substrates. A 2 nm thick metal Pt film was deposited by argon-ion sputtering onto a PyC film on a SiO$_2$/Si substrate.[44] The Pt film was annealed for 1 hour at 500 °C in a quartz-tube furnace with a localised high saturation of S vapour and a 150 sccm 10% H$_2$/Ar flow at 300 mbar (see Fig. 1(a)). This arrangement was based on the nested configuration described by Xu et al.[36] An additional local sulfur charge is placed at the mouth of the inner tube, at the edge of the primary hot-zone, to increase the S vapour concentration within. Previous research has shown that at lower pressure, or lower sulfur content, films with PtS stoichiometry are obtained.[35] This simple method avoids the need for exotic, expensive or hazardous precursors and is essentially a scalable process suitable for producing large-area polycrystalline films.

High-resolution XPS, Raman spectroscopy and X-ray diffraction (XRD) were utilised to confirm the synthesis of PtS$_2$. The characteristic XPS core-levels for PtS$_2$ are the Pt 4f and the S 2p (see Fig. 1(b) and (c)), both regions show dominant doublet pairs corresponding to PtS$_2$. The Pt 4f$_{7/2}$ peak is centred at 73.9 eV while the S 2p$_{3/2}$ is at 162.2 eV, consistent with the expected values.[48] From the fitting, the small shoulder at ~72 eV is attributed to a low level of Pt(II) contribution. Comparing the relative peak areas of the PtS$_2$ components yields a stoichiometry of PtS$_{1.89}$.[36] As noted earlier, a lack of sulfur during synthesis will result in the synthesis of PtS, but despite evidence of an excess of elemental sulfur, there are still indications of trace PtS present in the films. The formation of polycrystalline PtS$_2$ is also supported by XRD of the thin-film, as shown in Fig. S1 of the ESI.†

Raman spectroscopy using 532 nm excitation yielded the spectrum shown in Fig. 1(d). PtS$_2$ has three main characteristic Raman modes, all of which are clearly distinguishable in this spectrum. These are the out-of-plane E$_g^1$ mode at 303 cm^{-1} and the in-plane modes A$_{1g}^2$ and A$_{1g}^1$ at 343 and ~334 cm^{-1}, respectively. The small shoulder ~360 cm^{-1} is likely due to the polycrystalline nature of the film or the presence of PtS, as this feature is not observed for in the Raman spectra of exfoliated PtS$_2$.[24,31] Otherwise this spectrum is consistent
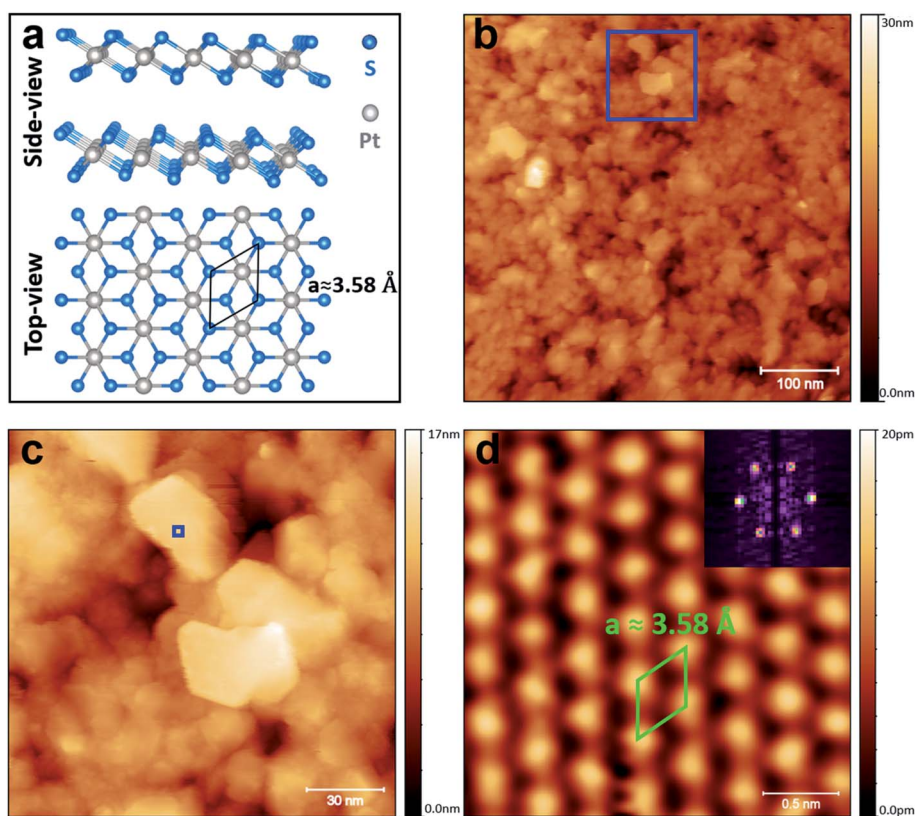

Fig. 2 STM images of PtS$_2$ film. (a) Structure model of 1T-PtS$_2$ with side- and top-views. (b) Large-scale STM image of the PtS$_2$ showing the polycrystalline film (500 × 500 nm^2, $V = 1.5$ V and $I = 120$ pA). (c) STM image of the area which is depicted in (b) (blue box), demonstrating flakes of PtS$_2$ with partially atomically-clean surface (150 × 150 nm^2, $V = 1.5$ V and $I = 120$ pA). (d) Atomically-resolved STM image, with FFT inset, of the 1T-PtS$_2$ surface indicates an interatomic distance of 3.58 ± 0.03 Å (2.5 × 2.5 nm^2, $V = 1.4$ V and $I = 400$ pA).

with high-purity PtS_2 with relatively small grain sizes yielding broader Raman peaks when compared to mechanically-exfoliated PtS_2.[24,31,36,49]

3.2. STM and STS characterisation of 1T-PtS_2

STM was used to investigate the atomic structure of the TAC-grown PtS_2 film as shown in Fig. 2. The 1T atomic-structure model of PtS_2 is schematically shown in Fig. 2(a) (side- and top-views). The large-area scan in Fig. 2(b) reveals that the films are polycrystalline consisting of crystalline grains (flakes) of PtS_2 with approximate lateral dimensions up to 40 nm. The root-mean square (RMS) roughness of the image 2(b) is around 2.6 nm. Overall, the surface morphology is similar to that of TAC-grown $PtSe_2$.[50,51] It can be seen from Fig. 2(c) (area depicted in Fig. 2(b) by the blue square) that there are some atomically-clean areas on the surface of the flakes, as can be judged from the sharp straight edges of the flakes. This indicates the stability of the PtS_2 during transfer, under ambient conditions, from the growth furnace to the STM chamber, which is in contrast with the behaviour of some 2D materials such as black phosphorous.[52] However, some contamination is present on the surface, most likely due to the exposure to ambient conditions. The crystal angles observed advocate hexagonal symmetry, which implies the presence of PtS_2, rather than cubic symmetry, which would suggest a significant presence of PtS.[35,53] Fig. 2(d)

displays an atomic-resolution image of the defect-free PtS_2 surface (area indicated by the blue square in Fig. 2(c)), verifying the 1T crystal structure of the PtS_2 grains.[24,36] The in-plane interatomic distance and a monolayer step height for the PtS_2 of 3.58 ± 0.03 Å and 5.5 ± 0.06 Å, respectively were obtained from this atomically-resolved STM images which is in good agreement with previous theoretical and experimental reports.[24,27,30,32,54] The Fast Fourier Transform (FFT) of the atomically resolved STM image is presented in inset of Fig. 2(d): the surface exhibits clearly ordered structures with the (1×1) symmetry of PtS_2. The spatial periodicity of $a = 3.58$ Å in the PtS_2 crystal was measured from FFT. It should be noted that no surface preparation under UHV (annealing or ion sputtering) was carried out prior to STM/STS investigation.

In order to understand the electronic nature of the TAC-grown PtS_2, STS was used to map the local density of states (LDOS) on the pristine surface of PtS_2. A large-scale STM image showing grains of PtS_2 is shown in Fig. 3(a). The inset in Fig. 3(a) shows the line profile of the PtS_2 flake (around 3.8 nm) where STS measurements were performed. It should be noted that thickness of the flake is an approximation since STM measures the density of states. Fig. 3(b) shows a high-resolution STM image (4×4 nm^2) of the atomically clean PtS_2 surface. Fig. 3(c) illustrates grid STS[55] measurements performed on the same area as in Fig. 3(b). 40×40 individual $I(V)$ measurements were
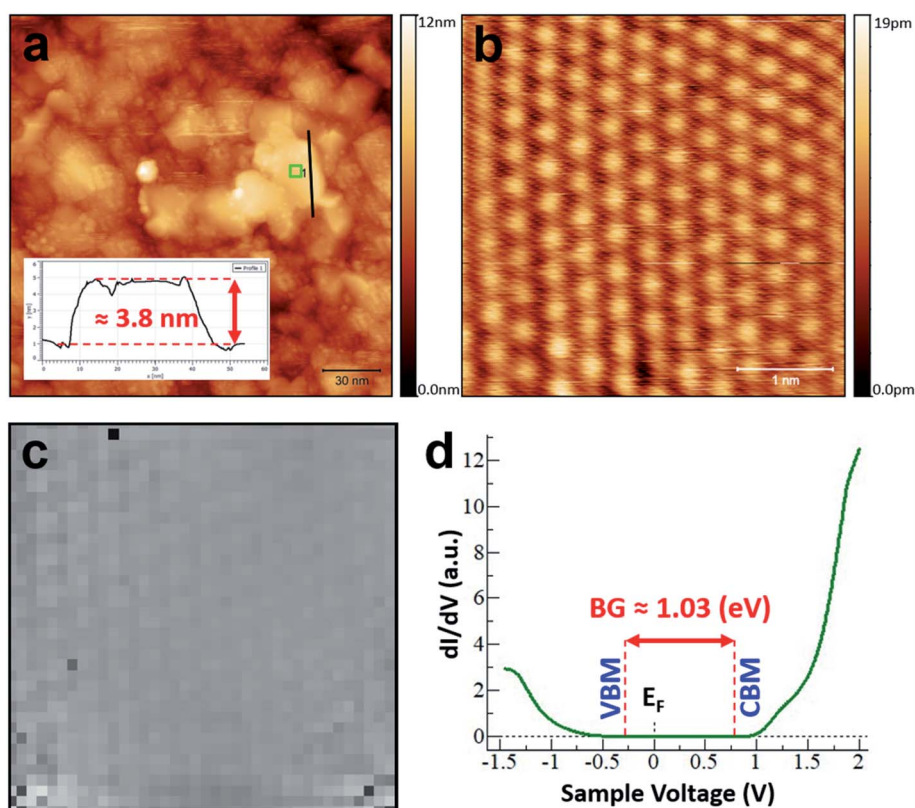

Fig. 3 STS of PtS_2 film. (a) Large-area STM image with ~3.8 nm thick flake of PtS_2 where STS analysis was performed. (b) Atomically-resolved STM image of the PtS_2 surface (4×4 nm^2, $V = 1.4$ V and $I = 400$ pA). A grid spectroscopy measurement was performed on the area depicted in (b). (c) 40×40 point grid spectroscopy measurement demonstrates the tunneling current value (taken from the $I(V)$) at each spectroscopy point on the grid at a bias voltage value of -1.45 V. (d) An averaged dI/dV spectra of the whole grid, which indicates that the bandgap is around 1.03 (eV).

conducted on the grid with dimensions of 4×4 nm^2. At each point of the grid, the spectra were averaged over three individual $I(V)$-measurements. The tip was moved in constant-current mode with the scanning parameters $V = 1.4$ (V) and $I = 400$ (pA) between points. The small variation observed in the tunnelling current at different voltages is due to differences in the electronic structure. The voltage was swept between -1.45 V and $+2$ V. Fig. 3(c) represents the tunnelling current from the $I(V)$ at each spectroscopy point at a bias voltage value of -1.45 V. Slightly brighter points correspond to a higher tunnelling current value at -1.45 V. A pixelated outline of the atomically-resolved features can be observed from the grid STS in Fig. 3(c).

It is known that dI/dV spectra (numerical derivative of $I(V)$) are proportional to the LDOS. The averaged dI/dV spectrum, which was acquired on the pristine terrace of PtS$_2$, is depicted in Fig. 3(d). The spectrum shown is an average of a few thousand individual spectra on the atomically clean surface. The VBM is positioned at 0.27 ± 0.02 eV below the Fermi level, and the CBM is positioned at 0.76 ± 0.02 eV above the Fermi level. Thus, the obtained bandgap of PtS$_2$ here is around 1.03 (eV), which is slightly larger than the bandgap predicted for this thickness in theoretical studies.[25,56] The LDOS of the PtS$_2$ flake is sharp in the conduction band, while in the valence band the LDOS increases gradually. The relative location of the Fermi level with respect to the CBM and VBM reveals p-type semiconducting behaviour for our PtS$_2$ flake.[23,25] Such a bandgap would be suitable for many applications including thermoelectric devices[31] and infrared photodetectors.[27,28] The beauty of this material is that the bandgap can be tuned by controlling the thickness of the PtS$_2$ film. Additionally, low-temperature synthesis of the PtS$_2$ allows growth on diverse substrates, such as glass and polyimide,[51,57] and thus broadens the potential application area. Our results establish that STM and STS are powerful techniques that can be applied to the characterisation of TAC-grown PtS$_2$.

4. Conclusions

Our results verify that PtS$_2$ can be preferentially grown by the TAC process and we have demonstrated that STM-based techniques can be applied to selectively investigate the atomic structure and electronic properties of polycrystalline PtS$_2$ films synthesised in this way. XPS, XRD and Raman spectroscopy confirmed the successful growth of PtS$_2$ with the correct stoichiometry. STM measurements allowed us to resolve the crystal structure of the TAC-grown PtS$_2$ and determine a lattice constant of 3.58 ± 0.03 Å. The bandgap for a flake with thicknesses 3.8 nm, obtained via STS measurements, was found to be 1.03 eV. The relative position of the Fermi level indicated p-type semiconducting behaviour. These fundamental results can contribute to future studies focused on PtS$_2$ and its application in devices.

Conflicts of interest

There are no conflicts to declare.

References

1 K. S. Novoselov, A. K. Geim, S. V. Morozov, D. Jiang, Y. Zhang, S. V. Dubonos, I. V. Grigorieva and A. A. Firsov, Electric Field Effect in Atomically Thin Carbon Films, *Science*, 2004, **306**, 666–669.

2 C. Rubio-Verdú, A. M. García-García, H. Ryu, D.-J. Choi, J. Zaldívar, S. Tang, B. Fan, Z.-X. Shen, S.-K. Mo, J. I. Pascual and M. M. Ugeda, Visualization of multifractal superconductivity in a two-dimensional transition metal dichalcogenide in the weak disorder regime, *Nano Lett.*, 2020, **20**(7), 5111–5118.

3 Y. Chen, W. Ruan, M. Wu, S. Tang, H. Ryu, H.-Z. Tsai, R. Lee, S. Kahn, F. Liou, C. Jia, O. R. Albertini, H. Xiong, T. Jia, Z. Liu, J. A. Sobota, A. Y. Liu, J. E. Moore, Z.-X. Shen, S. G. Louie, S.-K. Mo and M. F. Crommie, Strong correlations and orbital texture in single-layer 1T-TaSe$_2$, *Nat. Phys.*, 2020, **16**, 218–224.

4 V. Yu. Aristov, A. N. Chaika, O. V. Molodtsova, S. V. Babenkov, A. Locatelli, T. O. Menteș, A. Sala, D. Potorochin, D. Marchenko, B. Murphy, B. Walls, K. Zhussupbekov and I. V. Shvets, Layer-by-Layer Graphene Growth on β-SiC/Si(001), *ACS Nano*, 2019, **13**(1), 526–535.

5 B. Anasori, M. Lukatskaya and Y. Gogotsi, 2D metal carbides and nitrides (MXenes) for energy storage, *Nat. Rev. Mater.*, 2017, **2**, 16098.

6 V. Vyas, F. Haase, L. Stegbauer, *et al.*, A tunable azine covalent organic framework platform for visible light-induced hydrogen generation, *Nat. Commun.*, 2015, **6**, 8508.

7 S. Goswami, S. Goswami and T. Venkatesan, An organic approach to low energy memory and brain inspired electronics, *Appl. Phys. Rev.*, 2020, **7**, 021303.

8 S. Z. Butler, S. M. Hollen, L. Cao, Yi Cui, J. A. Gupta, H. R. Gutiérrez, T. F. Heinz, S. S. Hong, J. Huang, A. F. Ismach, E. J. Halperin, M. Kuno, V. V. Plashnitsa, R. D. Robinson, R. S. Ruoff, S. Salahuddin, J. han, Li Shi, M. G. Spencer, *et al.*, Progress, Challenges, and Opportunities in Two-Dimensional Materials Beyond Graphene, *ACS Nano*, 2013, **7**(no. 4), 2898–2926.

9 B. Schuler, D. Y. Qiu, S. Refaely-Abramson, C. Kastl, C. T. Chen, S. Barja, R. J. Koch, D. F. Ogletree, S. Aloni, A. M. Schwartzberg, J. B. Neaton, S. G. Louie and A. Weber-

Bargioni, Large Spin-Orbit Splitting of Deep In-Gap Defect States of Engineered Sulfur Vacancies in Monolayer WS$_2$, *Phys. Rev. Lett.*, 2019, **123**(7), 076801.

10 D. Edelberg, D. Rhodes, A. Kerelsky, B. Kim, J. Wang, A. Zangiabadi, C. Kim, A. Abhinandan, J. Ardelean, M. Scully, D. Scullion, L. Embon, R. Zu, E. J. G. Santos, L. Balicas, C. Marianetti, K. Barmak, X. Zhu, J. Hone and A. N. Pasupathy, Approaching the Intrinsic Limit in Transition Metal Diselenides *via* Point Defect Control, *Nano Lett.*, 2019, **19**(no. 7), 4371–4379.

11 S. Barja, S. Refaely-Abramson, B. Schuler, *et al.*, Identifying substitutional oxygen as a prolific point defect in monolayer transition metal dichalcogenides, *Nat. Commun.*, 2019, **10**, 3382.

12 L. Ansari, S. Monaghan, N. McEvoy, C. Ó Coileáin, C. P. Cullen, J. Lin, R. Siris, T. Stimpel-Lindner, K. F. Burke, G. Mirabelli, R. Duffy, E. Caruso, R. E. Nagle, G. S. Duesberg, P. K. Hurley and F. Gity, Quantum confinement-induced semimetal-to-semiconductor evolution in large-area ultra-thin PtSe$_2$ films grown at 400 °C, *npj 2D Mater. Appl.*, 2019, **3**, 33.

13 H. Ma, P. Chen, B. Li, J. Li, R. Ai, Z. Zhang, G. Sun, K. Yao, Z. Lin, B. Zhao, R. Wu, X. Tang, X. Duan and X. Duan, Thickness-Tunable Synthesis of Ultrathin Type-II Dirac Semimetal PtTe$_2$ Single Crystals and Their Thickness-Dependent Electronic Properties, *Nano Lett.*, 2018, **18**(no. 6), 3523–3529.

14 S. Manzeli, D. Ovchinnikov, D. Pasquier, O. V. Yazyev and A. Kis, 2D transition metal dichalcogenides, *Nat. Rev. Mater.*, 2017, **2**, 17033.

15 Z. Pedramrazi, C. Herbig, A. Pulkin, S. Tang, M. Phillips, D. Wong, H. Ryu, M. Pizzochero, Y. Chen, F. Wang, E. J. Mele, Z.-X. Shen, S.-K. Mo, O. V. Yazyev and M. F. Crommie, Manipulating Topological Domain Boundaries in the Single-Layer Quantum Spin Hall Insulator 1T′–WSe$_2$, *Nano Lett.*, 2019, **19**(no. 8), 5634–5639.

16 Q. Wang, K. Kalantar-Zadeh, A. Kis, J. N. Coleman and M. S. Strano, Electronics and optoelectronics of two-dimensional transition metal dichalcogenides, *Nat. Nanotechnol.*, 2012, **7**, 699–712.

17 N. Rohaizad, C. C. Mayorga-Martinez, Z. Sofer, R. D. Webster and M. Pumera, Layered platinum dichalcogenides (PtS$_2$, PtSe$_2$, PtTe$_2$) for non-enzymatic electrochemical sensor, *Appl. Mater. Today*, 2020, 100606.

18 J. B. McManus, D. Horvath, M. Browne, C. P Cullen, G. Cunningham, T. Hallam, K. Zhussupbekov, D. Mullarkey, C. O. Coileain, I. V. Shvets, M. Pumera, G. S. Duesberg and N. McEvoy, Low-temperature synthesis and electrocatalytic application of large-area PtTe$_2$ thin films, *Nanotechnology*, 2020, **31**(37), 375601.

19 R. Kempt, A. Kuc and T. Heine, Two-Dimensional Noble-Metal Chalcogenides and Phosphochalcogenides, *Angew. Chem., Int. Ed.*, 2020, **59**, 9242–9254.

20 Y.-H. Lee, X.-Q. Zhang, W. Zhang, M.-T. Chang, C.-T. Lin, K.-D. Chang, Y.-C. Yu, J. T.-W. Wang, C.-S. Chang, L.-J. Li and T.-W. Lin, Synthesis of Large-Area MoS$_2$ Atomic Layers

with Chemical Vapor Deposition, *Adv. Mater.*, 2012, **24**(no. 17), 2320–2325.

21 C.-P. Lu, G. Li, J. Mao, L.-M. Wang and E. Y. Andrei, Bandgap, Mid-Gap States, and Gating Effects in MoS$_2$, *Nano Lett.*, 2014, **14**(no. 8), 4628–4633.

22 X. Chia, A. Adriano, P. Lazar, Z. Sofer, J. Luxa and M. Pumera, Layered Platinum Dichalcogenides (PtS$_2$, PtSe$_2$, and PtTe$_2$) Electrocatalysis: Monotonic Dependence on the Chalcogen Size, *Adv. Funct. Mater.*, 2016, **26**, 4306–4318.

23 D. Zhao, S. Xie, Y. Wang, H. Zhu, L. Chen, Q. Sun and D. W. Zhang, Synthesis of large-scale few-layer PtS$_2$ films by chemical vapor deposition, *AIP Adv.*, 2019, **9**, 025225.

24 Y. Zhao, J. Qiao, P. Yu, Z. Hu, Z. Lin, S. P. Lau, Z. Liu, W. Ji and Y. Chai, Extraordinarily Strong Interlayer Interaction in 2D Layered PtS$_2$, *Adv. Mater.*, 2016, **28**, 2399–2407.

25 R. A. B. Villaos, C. P. Crisostomo, Z. Huang, S.-M. Huang, A. A. B. Padama, M. A. Albao, H. Lin and F.-C. Chuang, Thickness dependent electronic properties of Pt dichalcogenides, *npj 2D Mater. Appl.*, 2019, **3**, 2.

26 K. Iordanidou, M. Houssab and C. Perssona, Carrier-mediated ferromagnetism in two-dimensional PtS$_2$, *RSC Adv.*, 2020, **10**, 952–957.

27 L. Li, W. Wang, Y. Chai, H. Li, M. Tian and T. Zhai, Few-Layered PtS$_2$ Phototransistor on h-BN with High Gain, *Adv. Funct. Mater.*, 2107, **27**, 1701011.

28 J. Yuan, T. Sun, Z. Hu, W. Yu, W. Ma, K. Zhang, B. Sun, S. P. Lau, Q. Bao, S. Lin and S. Li, Wafer-Scale Fabrication of Two-Dimensional PtS$_2$/PtSe$_2$ Heterojunctions for Efficient and Broad band Photodetection, *ACS Appl. Mater. Interfaces*, 2018, **10**(47), 40614–40622.

29 L. Cai, N. Zhang, B. Qiu and Y. Chai, Computational Design of Transition Metal Single Atom Electrocatalysts on PtS$_2$ for Efficient Nitrogen Reduction, *ACS Appl. Mater. Interfaces*, 2020, **12**(18), 20448–20455.

30 H. L. Zhuang and R. G. Hennig, Computational Search for Single-Layer Transition-Metal, *J. Phys. Chem. C*, 2013, **117**, 20440–20445.

31 L. Pi, L. Li, X. Hu, S. Zhou, H. Li and T. Zhai, Temperature dependence of Raman responses of few-layer PtS$_2$, *Nanotechnology*, 2018, **29**, 505709.

32 H. Long, C. Y. Tang, P. K. Cheng, X. Y. Wang, W. Qarony and Y. H. Tsang, Ultrafast laser pulses generation by using 2D layered PtS$_2$ as a saturable absorber, *J. Lightwave Technol.*, 2019, **37**, 1174–1179.

33 E. Davy Esq., On the combinations of sulphur and phosphorus with platina, *Philos. Mag.*, 1812, **VII**, 27–39.

34 F. Gronvold, H. Haraldsen and A. Kjekshus, On the Sulfides, Selenides and Tellurides of Platinum, *Acta Chem. Scand.*, 1960, **14**, 1879–1893.

35 J. Huang, N. Dong, N. McEvoy, L. Wang, C. Ó. Coileáin, H. Wang, C. P. Cullen, C. Chen, S. Zhang, L. Zhang and J. Wang, Surface-State Assisted Carrier Recombination and Optical Nonlinearities in Bulk to 2D Nonlayered PtS, *ACS Nano*, 2019, **13**(11), 13390–13402.

36 H. Xu, H.-P. Huang, H. F. Fei, J. Feng, H.-R. Fuh, J. Cho, M. Choi, Y. Chen, L. Zhang, D. Chen, D. Zhang, C. Ó. Coileáin, X. Han, C.-R. Chang and H.-C. Wu, Strategy

for Fabricating Wafer-Scale Platinum Disulfide, *ACS Appl. Mater. Interfaces*, 2019, **11**(8), 8202–8209.

37 H. P. Komsa, S. Kurasch, O. Lehtinen, U. Kaiser and A. V. Krasheninnikov, From point to extended defects in two-dimensional MoS_2: evolution of atomic structure under electron irradiation, *Phys. Rev. B: Condens. Matter Mater. Phys.*, 2013, **88**, 035301.

38 J. Hong, Z. Hu, M. Probert, K. Li, D. Lv, X. Yang, L. Gu, N. Mao, Q. Feng, L. Xie, J. Zhang, D. Wu, Z. Zhang, C. Jin, W. Ji, X. Zhang, J. Yuan and Z. Zhang, Exploring atomic defects in molybdenum disulphide monolayers, *Nat. Commun.*, 2015, **6**, 6293.

39 S. Wang, A. Robertson and J. H. Warner, Atomic structure of defects and dopants in 2D layered transition metal dichalcogenides, *Chem. Soc. Rev.*, 2018, **47**, 6764–6794.

40 J. Osing and I. V. Shvets, Bulk defects in graphite observed with a scanning tunnelling microscope, *Surf. Sci.*, 1998, **417**(no. 1), 145–150.

41 H. Zheng, Y. Choi, F. Baniasadi, D. Hu, L. Jiao, K. Park and C. Tao, Visualization of point defects in ultrathin layered 1T-$PtSe_2$, *2D Mater.*, 2019, **6**, 041005.

42 A. S. Frolov, A. S. Frolov, J. Sánchez-Barriga, C. Callaert, J. Hadermann, A. V. Fedorov, D. Yu. Usachov, A. N. Chaika, B. C. Walls, K. Zhussupbekov, I. V. Shvets, M. Muntwiler, M. Amati, L. Gregoratti, A. Yu. Varykhalov, O. Rader and L. V. Yashina, Atomic and Electronic Structure of a Multidomain GeTe Crystal, *ACS Nano*, 2020, DOI: 10.1021/acsnano.0c05851.

43 C. Xie, S. Jiang, Y. Gao, M. Hong, S. Pan, J. Zhao and Y. Zhang, Giant Thickness-Tunable Bandgap and Robust Air Stability of 2D Palladium Diselenide, *Small*, 2020, **16**, 2000754.

44 N. McEvoy, N. Peltekis, S. Kumar, E. Rezvani, H. Nolan, G. P. Keeley, W. J. Blau and G. S. Duesberg, Synthesis and analysis of thin conducting pyrolytic carbon films, *Carbon*, 2012, **50**(3), 1216–1226.

45 C. Dong, G. Meng, S. E. Saji, X. Gao, P. Zhang, D. Wu, Yi Pan, Z. Yin and Y. Cheng, Simulation-guided nanofabrication of high-quality practical tungsten probes, *RSC Adv.*, 2020, **10**, 24280–24287.

46 H. R. Gutiérrez, N. Perea-López, A. L. Elías, A. Berkdemir, B. Wang, R. Lv, F. López-Urías, V. H. Crespi, H. Terrones and M. Terrones, Extraordinary Room-Temperature Photoluminescence in Triangular WS_2 Monolayers, *Nano Lett.*, 2013, **13**(no. 8), 3447–3454.

47 C. Yim, K. Lee, N. McEvoy, M. O'Brien, S. Riazimehr, N. C. Berner, C. P. Cullen, J. Kotakoski, J. C. Meyer, M. C. Lemme and G. S. Duesberg, High-Performance Hybrid Electronic Devices from Layered $PtSe_2$ Films Grown at Low Temperature, *ACS Nano*, 2016, **10**(no. 10), 9550–9558.

48 J. Dembowski, L. Marosi and M. Essig, Platinum Disulfide by XPS, *Surf. Sci. Spectra*, 1993, **2**, 133–137.

49 D. Caffrey, A. Zhussupbekova, R. K. Vijayaraghavan, A. Ainabayev, A. Kaisha, G. Sugurbekova, I. V. Shvets and K. Fleischer, Crystallographic Characterisation of Ultra-Thin, or Amorphous Transparent Conducting Oxides—The Case for Raman Spectroscopy, *Materials*, 2020, **13**(no. 2), 267.

50 C. Yim, V. Passi, M. C. Lemme, G. S. Duesberg, C. Ó Coileáin, E. Pallecchi, D. Fadil and N. McEvoy, Electrical devices from top-down structured platinum diselenide films, *npj 2D Mater. Appl.*, 2018, **2**, 5.

51 C. S. Boland, C. Ó. Coileáin, S. Wagner, J. B. McManus, C. P. Cullen, M. C. Lemme, G. S. Duesberg and N. McEvoy, $PtSe_2$ grown directly on polymer foil for use as a robust piezoresistive sensor, *2D Materials*, 2019, **6**(4), 045029.

52 J. O. Island, G. A. Steele, H. S. J. van der Zant and A. Castellanos-Gomez, Environmental instability of few-layer black phosphorus, *2D Materials*, 2015, **2**(1), 011002.

53 V. I. Rozhdestvina, A. A. Udovenko, S. V. Rubanov and N. V. Mudrovskaya, Structural Investigation of Cooperite (PtS) Crystals, *Crystallogr. Rep.*, 2016, **61**, 193–202.

54 S. Furuseth, K. Selte and A. Kjekshus, Redetermined crystal structures of $NiTe_2$, $PdTe_2$, PtS_2, $PtSe_2$, and $PtTe_2$, *Acta Chem. Scand.*, 1065, **19**, 257–258.

55 K. Zhussupbekov, K. Walshe, S. I. Bozhko, A. Ionov, K. Fleischer, E. Norton, A. Zhussupbekova, V. Semenov, I. V. Shvets and B. Walls, Oxidation of Nb(110): atomic structure of the NbO layer and its influence on further oxidation, *Sci. Rep.*, 2020, **10**, 3794.

56 S. Liu, H. Zhu, Z. Liu and G. Zhou, Symmetrical metallic and magnetic edge states of nanoribbon from semiconductive monolayer PtS_2, *Phys. Lett. A*, 2018, **382**(no. 11), 776–780.

57 E. Okogbue, S. S. Han, T.-J. Ko, H.-S. Chung, J. Ma, M. S. Shawkat, J. H. Kim, J. H. Kim, E. Ji, K. H. Oh, L. Zhai, G.-H. Lee and Y. Jung, Multifunctional Two-Dimensional $PtSe_2$-Layer Kirigami Conductors with 2000% Stretchability and Metallic-to-Semiconducting Tunability, *Nano Lett.*, 2019, **19**(no. 11), 7598–7607.